Molecular Basis for the Protein Recognition Specificity of the Dynein Light Chain DYNLT1/Tctex1
CHARACTERIZATION OF THE INTERACTION WITH ACTIVIN RECEPTOR IIB*

Javier Merino-Gracia[‡1], Héctor Zamora-Carreras[§2], Marta Bruix[§], and Ignacio Rodríguez-Crespo[‡3]

From the ‡Departamento Bioquímica y Biología Molecular, Facultad de Ciencias Químicas, Universidad Complutense de Madrid, 28040 Madrid, Spain and §Departamento Química Física Biológica, Instituto Química Física Rocasolano, Consejo Superior de Investigaciones Científicas, Serrano 119, 28006 Madrid, Spain

It has been suggested that DYNLT1, a dynein light chain known to bind to various cellular and viral proteins, can function both as a molecular clamp and as a microtubule-cargo adapter. Recent data have shown that the DYNLT1 homodimer binds to two dynein intermediate chains to subsequently link cargo proteins such as the guanine nucleotide exchange factor Lfc or the small GTPases RagA and Rab3D. Although over 20 DYNLT1-interacting proteins have been reported, the exact sequence requirements that enable their association to the canonical binding groove or to the secondary site within the DYNLT1 surface are unknown. We describe herein the sequence recognition properties of the hydrophobic groove of DYNLT1 known to accommodate dynein intermediate chain. Using a pepscan approach, we have substituted each amino acid within the interacting peptide for all 20 natural amino acids and identified novel binding sequences. Our data led us to propose activin receptor IIB as a novel DYNLT1 ligand and suggest that DYNLT1 functions as a molecular dimerization engine bringing together two receptor monomers in the cytoplasmic side of the membrane. In addition, we provide evidence regarding a dual binding mode adopted by certain interacting partners such as Lfc or the parathyroid hormone receptor. Finally, we have used NMR spectroscopy to obtain the solution structure of human DYNLT1 forming a complex with dynein intermediate chain of ~74 kDa; it is the first mammalian structure available.

Transport of various intracellular cargoes along cytoskeleton filaments is essential for the morphogenesis and function of eukaryotic cells. Intracellular transport is mediated by cytoskeletal motors including kinesin, myosin, and dynein, which are typically linked to various cargoes by adaptor proteins. Dyneins are large microtubule-based molecular motors involved in diverse fundamental cellular processes including retrograde vesicular transport, mitotic spindle positioning, axonal transport, and ciliary/flagellar beating (1, 2). The cytoplasmic dynein motor is a multicomponent protein of ~1.6 MDa that contains two heavy (~530 kDa), two intermediate (DICs)[4] (~74-kDa), two light intermediate (~50–60-kDa), and three light (~8-, 14-, and 22-kDa) chains (2, 3). The two DICs bind directly to the heavy chains, and then three different homodimeric light chains bind to the intermediate chain at separate sites.

There are three known dynein light chain gene families that are components of cytoplasmic dynein (4): the Tctex family (DYNLT1 and DYNLT3), the LC8 family (DYNLL1 and DYNLL2), and the Roadblock family (DYNLRB1 and DYNLRB2). DYNLL1, a ubiquitous eukaryotic protein, is the most highly conserved among light chains and, interestingly, despite lacking sequence homology displays a 3D fold very similar to that of DYNLT1 (5–8). Homodimeric DYNLT1 binds to residues [151]SKVTQVDFL[159] whereas homodimeric DYNLL1 binds to residues [167]SKETQTP[173] (human sequences) of two parallel polypeptides of DIC holding them together (9–11). DYNLT1 and DYNLL1 are structural homologs, they bind to DIC consecutively, and their mode of interaction with target sequences is essentially identical, both functioning as molecular clamps (9, 10, 12). Crystal and NMR solution structures show that all recognition motifs presented by DYNLL1 partners bind in the same manner to two symmetrical grooves on the DYNLL1 homodimer with the ~10-amino acid recognition motifs incorporated as antiparallel β-strands (9, 12–14). On the contrary, the amount of available data regarding biochemical information of DYNLT1 is much more limited. Whereas homodimeric DYNLT1 can bind to dynein intermediate chain using its two symmetrical grooves and extending the preformed β-sheet with an additional β-strand as well (9, 10), it can also recognize protein targets through interactions with surface residues (15, 16).

With a growing list, DYNLT1 binders include over 20 polypeptides of both cellular and viral origin (17, 18). So far, no

[4] The abbreviations used are: DIC, dynein intermediate chain of ~74 kDa, specifically DYNC1I; ActRII, activin receptor II; DYNLL, dynein light chain of ~8 kDa, also known as DLC8 or LC8; DYNLT, dynein light chain of ~13 kDa, also known as Tctex (T-complex testis-specific protein) or DYNLT1; ITC, isothermal titration calorimetry; HSQC, heteronuclear single quantum coherence; GEF, guanine nucleotide exchange factor; FP, fluorescence polarization; TOCSY, total correlation spectroscopy.

consensus binding sequence for DYNLT1 when binding to its protein partners has yet been identified, and it is not even known whether they associate to the canonical binding groove or to the protein surface. The former situation would mean that DYNLT1 might function as a molecular dimerization engine, whereas the latter would imply that DYNLT1 might link these protein cargoes to the dynein motor for them to be transported. The two published crystal structures clearly established the exact amino acids within dynein intermediate chain that bind to the hydrophobic groove of DYNLT1. In the case of rat intermediate chain in complex with fly DYNLT1 (10), DIC residues KLGMAKITQVDFP insert within the DYNLT1 cavity with flanking amino acids establishing contacts with the solvent but not with the protein. Remarkably, this piece of data strongly contradicts published binding assays of DYNLT1 to several of its associated proteins. It has been suggested that, upon binding, DYNLT1 must recognize a polybasic motif such as (R/K)(R/K)XX(R/K). In this regard, site-directed mutagenesis studies have described how the binding of DYNLT1 to G protein β subunit (19), Doc2α (20), CD5 (21), or CT850 (22) is abrogated in the absence of these basic residues. To shed light on the binding mechanism of DYNLT1 to its protein targets, we have analyzed this association using a variety of techniques. We describe herein the sequence requirements that must be found in protein targets, we identify novel binding partners, and we report the solution structure of the first mammalian DYNLT1 in complex with a dynein intermediate chain peptide. Finally, we analyze the binding of the guanine nucleotide exchange factor Lfc to DYNLT1, proposing a dual binding mechanism and showing how the polybasic stretch contributes to the overall binding energy through interactions lying outside the consensus binding groove.

Results

The Polybasic Sequence Motifs of Mammalian Dynein Intermediate Chains Are Not Required for DYNLT1 Binding—In mammals, there are two intermediate chains per dynein complex with a molecular mass of ~74,000 Da known as DYNC1IC1 and DYNC1IC2 (4, 23, 24) (for clarity, we will refer to them as DIC1 and DIC2). Alternative splicing and phosphorylation produce multiple intermediate chain isoforms (23, 24). The binding sites for DYNLT1 and DYNLL1 light chains were found to be just C-terminal of the second alternative splice region in the intermediate chain gene (9, 10, 25). In addition, the binding sites for both light chains on the intermediate chain were found to be sequential (Fig. 1*A*). First, we wondered which is the minimal part of DIC capable of interacting with DYNLT1. Using a yeast two-hybrid assay, we could show that a short polypeptide of either isoform 1 or isoform 2 lacking the polybasic stretch was able to interact with DYNLT1 (Fig. 1*B*). Next, we expressed and purified recombinant DYNLT1 as well as a self-saturated DYNLT1 (see below) and analyzed whether they were properly folded using circular dichroism. Deconvolution of CD spectra revealed that both DYNLT1 in complex with a DIC1 peptide (KLGVSKVTQVDFLPREV) and its self-saturated DYNLT1 counterpart showed a very similar spectrum with calculated secondary structure elements of 25.2% α-helix, 10.8% antiparallel β-strand, 10.9% parallel β-strand, 18.5% β-turns,

and 34.6% random coil for the former and 24.9% α-helix, 10.9% antiparallel β-strand, 11.9% parallel β-strand, 18.5% β-turns, and 33.8% random coil for the latter (Fig. 1*C*). The CD spectrum of DYNLT1 is in agreement with previously reported data (26) and with the atomic information available. A thermodynamic analysis of the interaction of DYNLT1 with a DIC1 peptide was performed using isothermal titration calorimetry (ITC) resulting in a K_d of 6.06 $\pm$ 1.3 μM (Fig. 1*D*). To further analyze in detail the binding of this DIC1 short peptide to DYNLT1, we used fluorescence polarization measurements. Saturation curves were then created by applying increasing concentrations of the purified DYNLT1 domain and a fixed concentration of the probe. The K_d value between probe and DYNLT1 was determined to be 4.80 $\pm$ 0.5 μM (Fig. 1*E*). Taken together, our results indicate that a short oligopeptide corresponding to residues 147–162 of DIC1 binds to DYNLT1 with high affinity and that the polybasic stretch that precedes this stretch is dispensable for binding. This finding contrasts with previous reports that indicated that the interaction required this polybasic region (25).

NMR Solution Structure of Human DYNLT1 in Complex with DIC—Next, we decided to obtain 3D information about the binding of a human dynein intermediate chain segment to human DYNLT1. We proceeded to express in bacteria recombinant DYNLT1 self-saturated with a dynein intermediate chain sequence (Fig. 2*A*) to obtain information about the binding mode of interacting peptides that might occupy the canonical groove. We have previously characterized this DYNLT1-DIC2 construct in yeast two-hybrid and pulldown assays and we have shown that its behavior is similar to that of DYNLT1 when associated to dynein intermediate chain (16). We used a DIC2 stretch fused to DYNLT1 because it resulted in much better protein yield than a DIC1 construct (data not shown). First, we tested that the added C-terminal DIC2 portion acquired the dynamic regime of the DYNLT1 moiety by analyzing the ^{1}H-^{15}N heteronuclear NOE data (Fig. 2*B*). In fact, region GMAKITQVDF has the same mean NOE value as the core of the DYNLT1 part. This is clear evidence of the interaction of the DIC peptide with the globular DYNLT1 moiety as suggested by the conformational chemical shift analysis. On the contrary, residues corresponding to the linker and to the N terminus of the DIC moiety have low NOE values, indicating that these regions behave as flexible segments. Next, we used NMR to confirm the correct folding of the recombinant DYNLT1-DIC2 construct by comparing its 1D ^{1}H spectrum with that of DYNLT1 in the same conditions. In all cases, there was good signal dispersion, and the conservation of the deshielded signals at about −0.3 and −0.8 ppm (corresponding to the methyl signals of Ile[64] and Ile[25] of wild-type DYNLT1), respectively, clearly indicates that the 3D structure of DYNLT1 is conserved in the construct. The NMR spectral assignment was performed by following standard heteronuclear protocols. Secondary structure elements determined from the conformational shifts ($\Delta\delta$) data (Fig. 2*C*) indicate that they are maintained in the DYNLT1 part of the construct. Low $\Delta\delta$ values observed in the linker section denote a mostly unstructured region, whereas significant $\Delta\delta$ values characteristic of a β-strand are observed in the DIC segment. In addition, the
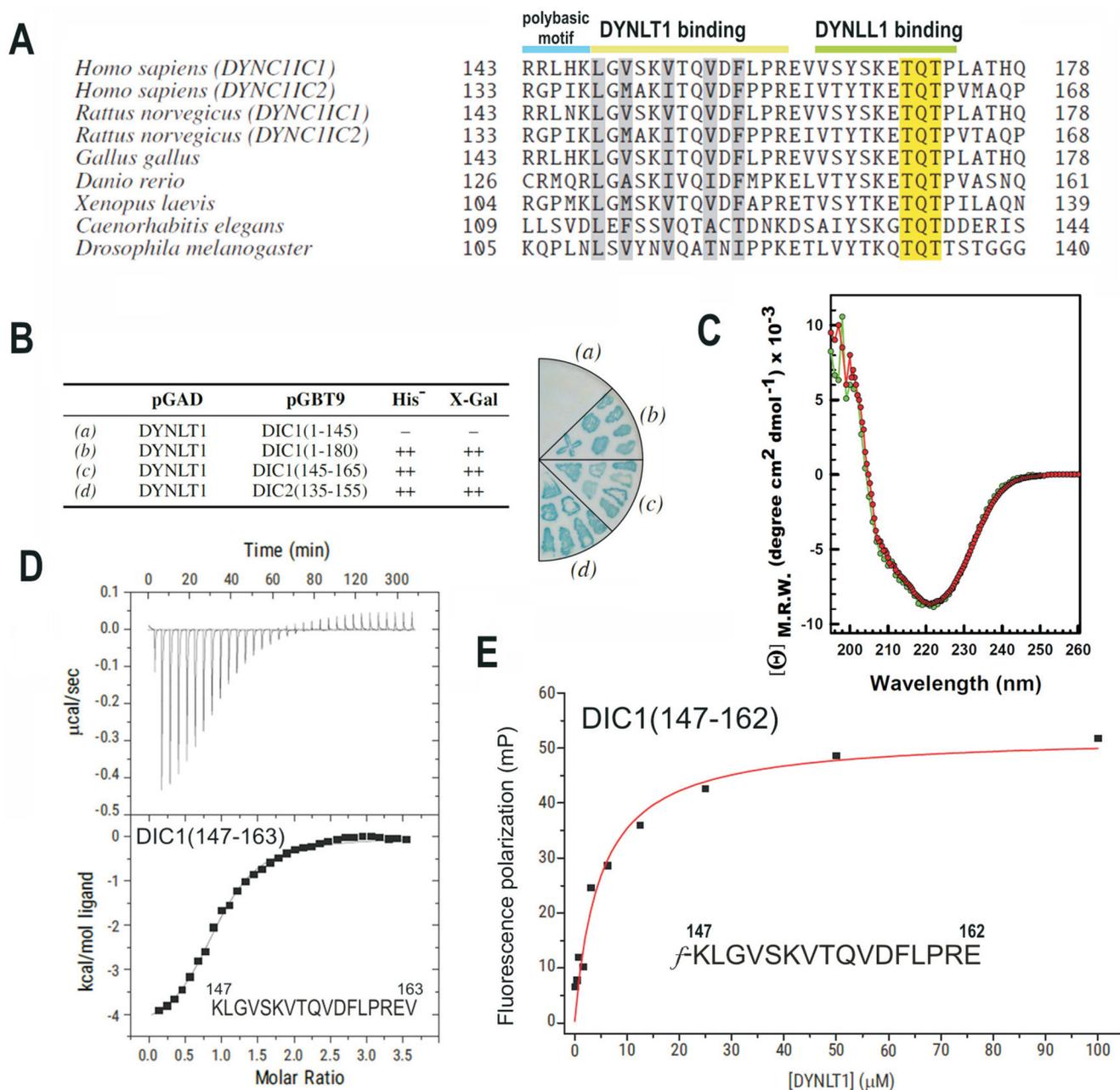
FIGURE 1. **Identification of the minimal DYNLT-binding region within dynein intermediate chain.** *A*, sequence comparison between mammalian DIC isoforms and those of selected model organisms known to bind DYNLT1 and DYNLL1 consecutively. The polybasic motif and the DYNLT1 and DYNLL1 binding sites are shown at the *top*. The characteristic TQT motif present in many DYNLL1 binding partners is also shown. *B*, yeast two-hybrid assay using DYNLT1 in the bait plasmid and various dynein intermediate chain constructs. Growth in the absence of the amino acid His and presence of 3-aminotriazole and X-Gal activity are shown. The *right panel* shows a representative result of an X-Gal assay in a plate. *C*, circular dichroism spectra of purified recombinant DYNLT1 saturated with a DIC1 peptide (KLGVSKVTQVDFLPREV) (in *red*) and its self-saturated DYNLT1-DIC2 counterpart (shown in *green*) in the far-UV region. *D*, ITC analysis of the binding of a dynein intermediate chain peptide (KLGVSKVTQVDFLPREV) to purified DYNLT1. The thermogram is shown in the *upper panel*, and the binding isotherm is shown in the *bottom panel*. Curve fitting rendered a K_d value of 6.06 ± 1.3 μM. *E*, representative binding curve for a FITC-labeled dynein intermediate chain peptide (*f*-KLGVSKVTQVDFLPRE) to DYNLT1 measured by fluorescence polarization. A calculated K_d of 4.80 ± 0.5 μM could be obtained. Results are representative of three independent experiments. *mP*, millipolarization units; M.R.W., mean residue weight.

assigned ^1H-^{15}N HSQC spectrum of DYNLT1-DIC2 and the amino acid assignment are shown in Fig. 2*D*.

3D Structure and Analysis of the Dimer Interface—Statistics of the calculation are summarized in Fig. 2*E*. A representative conformer of the DYNLT1-DIC2 structure determined by NMR is shown in Fig. 3*A*. The structure is a well defined β-strand-swapped dimer and maintains the same tertiary structure shown by other members of the DYNLT family. Each

monomer has two α-helices: α1, residues 14−29 and α2, residues 37−57. The β-strands are defined by the following residues: β1, 64−69; β2, 78−81; β3, 93−97; β4, 104−109; and β5, 140−142/144−148 (numbering according to UniProt P63172 and Q13409). The DIC2 sequences (one of each monomer) lie in the hydrophobic grooves on the structure surface, extending the central β-sheet, and are oriented in the same N to C terminus direction. This β-structure is better defined in two frag-
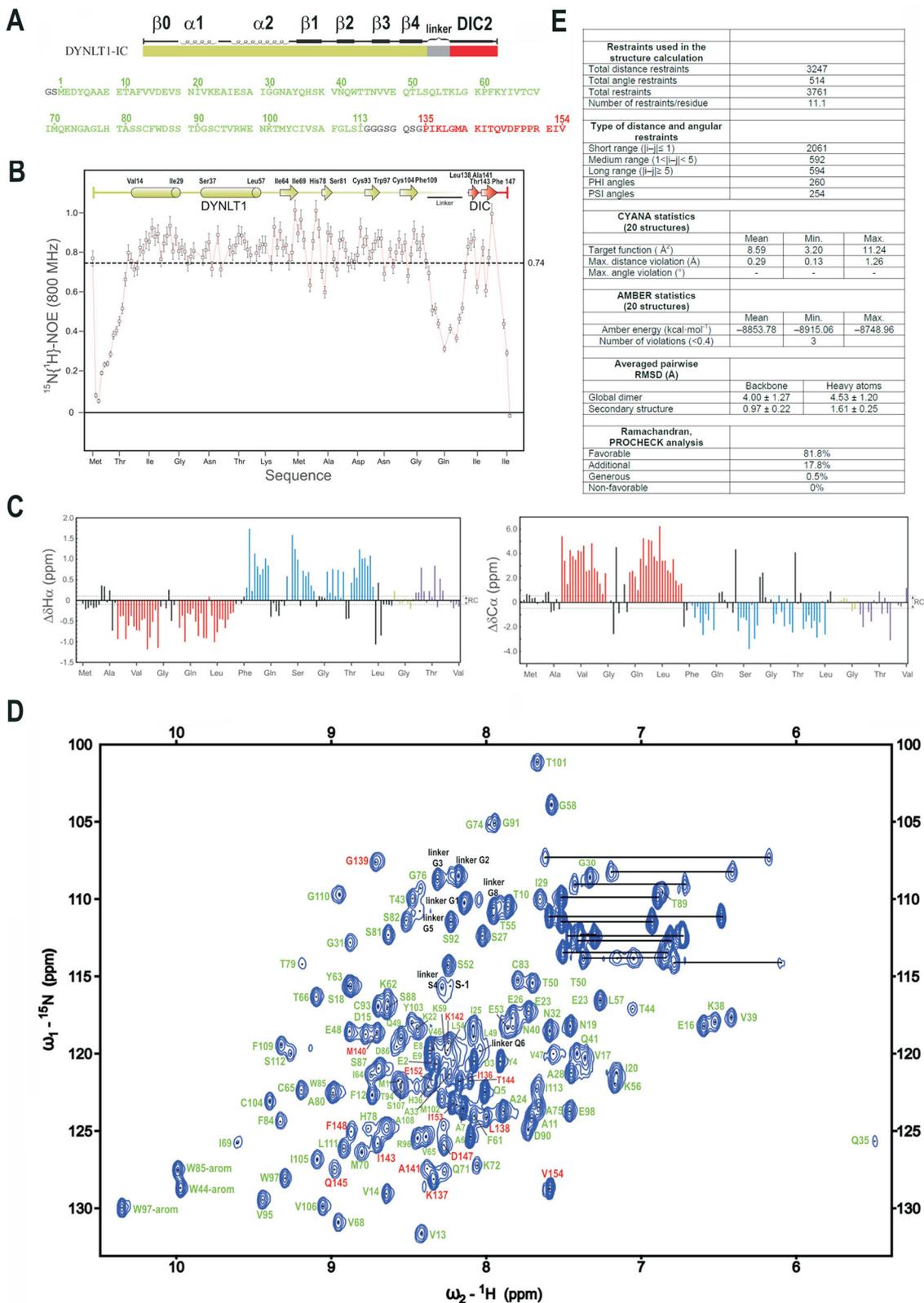
FIGURE 2. **NMR analysis of the DYNLT1-DIC2 chimera.** *A*, design of the chimeric construct in which a linker (in *gray*) connects DYNLT1 (in *green*) with a DIC2 fragment (in *red*). The amino acid sequence is also shown. Numbering corresponds to UniProt P63172 (full-length human DYNLT1, 113 amino acids) and UniProt Q13409 (human DIC2, residues 135–154). *B*, ^{1}H-^{15}N heteronuclear NOE data of the purified DYNLT1-DIC2 protein. Elements of secondary structure are represented on *top*. The *dotted line* represents the average value, which is indicated on the *right*. *C*, conformational shift ($\Delta\delta$) data obtained at 25 °C. *Dotted lines* represent the limit of the random coil values. *D*, ^{1}H-^{15}N HSQC spectrum of DYNLT1-DIC2. The amino acid assignment is also shown. Residues corresponding to DYNLT1 are shown in *green*, whereas those corresponding to the DIC2 part are shown in *red*. The remaining residues are shown in *black* as shown in *A*. *E*, summary of the statistics corresponding to the NMR calculations. *RMSD*, root mean square deviation. The *error bars* indicate 5% of the mean value.
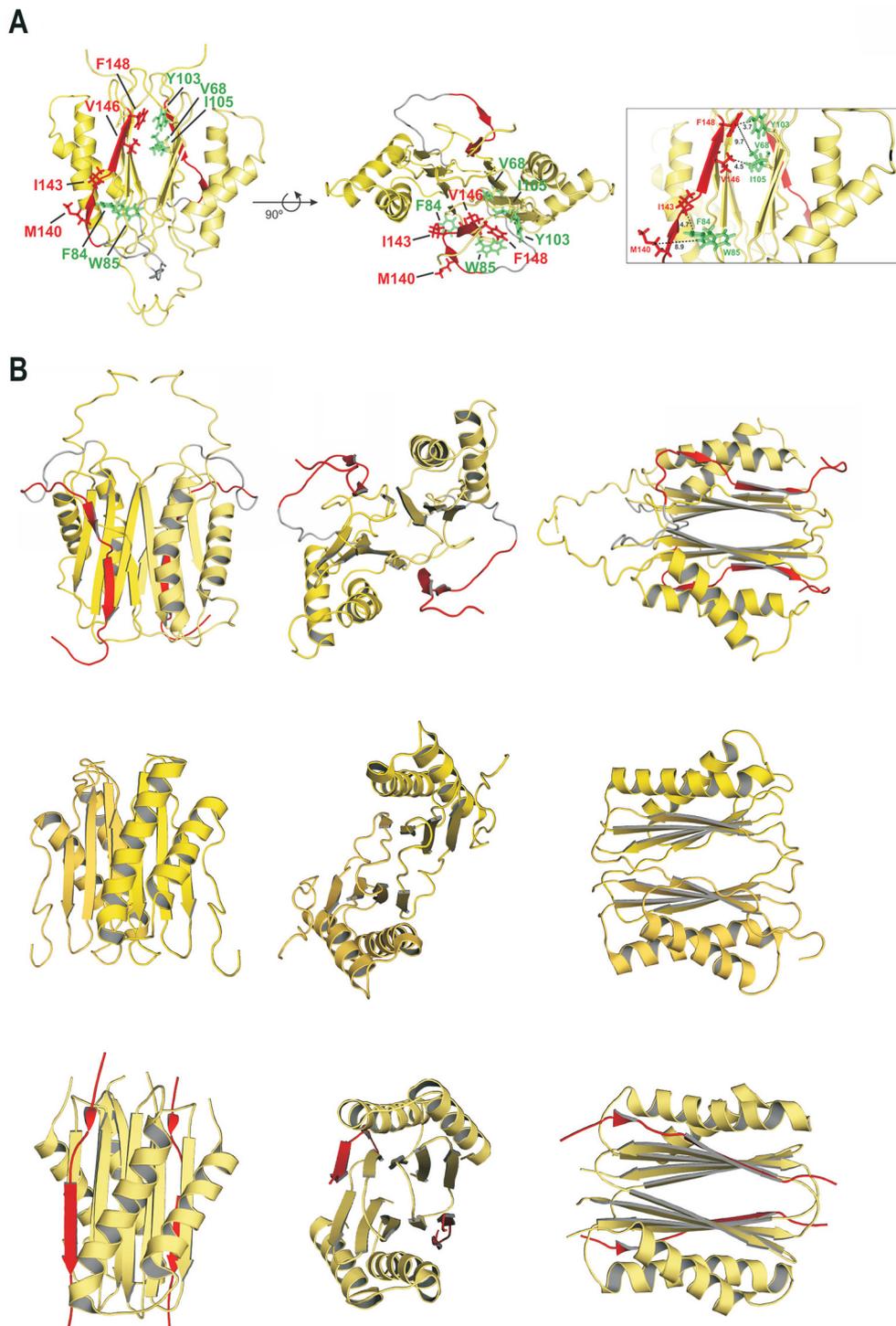
FIGURE 3. **Solution structure of human DYNLT1 self-saturated with a dynein intermediate chain polypeptide occupying the canonical binding groove.**
A, two different views of the calculated 3D structure of DYNLT1-DIC2 in a ribbon representation. The two chains of each DYNLT1 monomer are colored in *yellow*, and the DIC segment is highlighted in *red*. The preformed β-sheets of the monomer-monomer interaction surface become extended by swapped antiparallel β-strands, hence creating the binding surface for the incoming, kinked antiparallel β-strand of DIC. The hydrophobic contacts between the DIC segment (K**LGM**AK**I**TQ**V**D**F**P) and the DYNLT1 structure are also shown in a stick format. In the *left* view, the proposed contacts of DIC Val and Phe can be seen in the *upper* part of the molecule, whereas the DIC Leu, Met, and Ile are shown in the *lower* part of the molecule. Interacting DYNLT1 hydrophobic residues are shown in *green*. The *right* view represents a 90° rotation of the top view. The *boxed panel* to the *right* shows a close-up of the interacting residues as well as the observed distances in Å. *B*, structural comparison of the human, *Chlamydomonas reinhardtii*, and *D. melanogaster* DYNLT1 in complex with DIC peptides. The *top three panels* depict the solution structure of human DYNLT1 in complex with human DIC that we obtained using NMR spectroscopy in comparison with atomic structures of its orthologs of *C. reinhardtii* obtained by NMR spectroscopy (5) (Protein Data Bank code 1XDX) (*three middle panels*) and with the *D. melanogaster* crystal structure (10) (Protein Data Bank code 2PG1) (*three bottom panels*). Please note that the *C. reinhardtii* solution structure was obtained in the absence of interacting peptide.

ments of the DIC sequence: Met-Ala-Lys and Thr-Gln-Val-Asp-Phe. Position DIC2 Gly[139] shows φ and ψ values that are far from an ideal β-strand structure, and some structural distortion is also observed around DIC2 Ile[143]. The formation of a bulge in the DIC2 stretch was also verified in previously reported structures (9, 10, 27) in which the total extension of the β-strand was impeded by structural alterations around the central Ile position. Three hydrophobic contact areas in which the side chains of three DIC2 residues are accommodated have been previously observed in the *Drosophila melanogaster* DYNLT1 crystal structure (10). Likewise, analysis of our data indicates that DIC2 Leu, Met, and Ile do, in fact, interact with DYNLT1 in hydrophobic binding cavities. Conversely, the more C-terminal DIC2 Val and Phe side chains seem to be in a solvent-exposed zone in which only minor contacts with DYNTL1 are expected (only two DYNLT1 hydrophobic residues, one Phe and one Trp, can be found in their vicinity, within a 8–10-Å range) (Fig. 3A). Because the two binding sites of the DYNLT1 dimer molecule are identical, it is interesting to mention that the length of the artificial linker designed in the chimera allows the possible coexistence of two different conformational structures that are perfectly compatible with the observed restrictions used in the structural calculation. In one, the sequence of DIC2 extends the β-strand of its own monomer, whereas in the other conformation the chimeric end is inserted into the opposite side of the dimer, extending the β-sheet of the other monomer. This can be a possible explanation for some broad NMR signals observed in the spectra as this would imply the presence of two dimeric populations in solution. Unfortunately, both types of conformers are indistinguishable by NMR in the current conditions.

Although crystals of mouse apo-DYNLT1 have been obtained, diffraction was very weak (28). Conversely, *D. melanogaster* apo-DYNLT1 crystals diffracting at sufficient quality have been obtained. Unfortunately, the absence of a binding peptide to insert in the canonical groove induced the formation of an aberrant hexameric structure in which each homodimer sequestered polypeptides from an adjacent homodimer to occupy the binding site (28). NMR studies performed using mouse DYNLT1 titrated with a dynein intermediate chain peptide that included the polybasic stretch observed changes in the β2-strand and the α2/α3-loop although the exact binding mode of interaction for those peptides could not be obtained (25). Furthermore, NMR spectroscopy also indicated that titration of *Chlamydomonas* DYNLT1 with an intermediate chain peptide resulted in changes in chemical shifts whose mapping onto the molecular surface revealed that they do not occur along the intermonomer grooves but rather are all located at one end of the molecule (5). This significantly contrasts with the two crystal structures of DYNLT1 in complex with dynein intermediate chain available (9, 10). Human DYNLT1 in complex with DIC adopts a fold similar to that observed for both the *Chlamydomonas* (5) and fly complexes (9, 10) (Fig. 3B). In general, the fly complex obtained by protein crystallography is more compact than either of the solution structures obtained by NMR spectroscopy. In all cases, the incoming peptide adopts an antiparallel β-strand conformation that extends the preformed β-sheet albeit with a clear kink that disrupts the expected

hydrogen bond pattern (Fig. 3B and Refs. 10 and 27). This feature probably makes it more difficult to predict putative DYNLT1-binding proteins just from the amino acid sequence.

Identification of Novel DYNLT1-interacting Proteins Capable of Occupying the Canonical Hydrophobic Groove—As discussed earlier, no structural data are available for DYNLT1 in complex with any polypeptide chain besides dynein chain. To explore the sequence requirements that lead to the binding of cellular and viral peptides to the hydrophobic groove of DYNLT1, we performed a binding assay using the pepscan technique. A matrix of pentadecapeptides attached to a cellulose membrane through a spacer was created using the DIC1 sequence, and each position was substituted for each of the 20 natural amino acids. The substitutions of any amino acid by itself were encircled in blue, and these spots served as positive, internal controls (Fig. 4A). Incubation with recombinant DYNLT1 also revealed that residues at the N terminus (Lys) or C terminus (Arg) lie outside the binding groove, and essentially any amino acid could occupy those positions (Fig. 4A). Remarkably, there are five positions in human DIC1, those occupied by Leu[148], Val[150], Val[153], Val[156], and Phe[158], where only hydrophobic amino acids can be accepted. These five hydrophobic binding pockets were also identified in the NMR structure, and our results clearly demonstrate that they dictate the interaction of associated polypeptides. Although the DYNLT1 binding sites within DIC1 and DIC2 almost share the central K(I/V)TQVDF heptapeptide, our pepscan results show that the flanking residues found in DIC2 (Met, Ala, and Pro) are not pointedly favored over other amino acids. This might indicate that this conserved heptapeptide significantly contributes to the binding energy.

Next, we used a yeast two-hybrid assay in which we eliminated each of these five hydrophobic amino acids and confirmed that the binding was completely lost or significantly reduced (Fig. 4B). Conversely, certain positions of DIC1 seemed to accept a significant diversity of residues such as Gly[149], Gln[155], and even Leu[159] maintaining the binding to DYNLT1. Interestingly, a few substitutions rendered peptides with increased binding to DYNLT1, and although some of them were between conserved amino acids, the appearance of certain changes was hard to predict beforehand considering the nature of the amino acid side chains. This was the case for the G149E, G149T, K152A, K152P, K152Y, Q155H, Q155T, Q155Y, Q155R, and D157H substitutions. To confirm that these mutations were indeed tolerated, we created DIC mutants to be used in our yeast two-hybrid assay and confirmed that all these unexpected substitutions did indeed result in dynein intermediate chain sequences that interacted with DYNLT1 tightly (Fig. 4B). In accord with these results, we inspected sequence databases and looked for cellular proteins with putative DYNLT1 binding motifs based on qualitative inspection (Fig. 4C). We selected 15 proteins that, in general, matched with the required five hydrophobic residues at the specified positions and displayed residues that were compatible with our pepscan results. Future experiments will certainly determine whether these polypeptide stretches of proposed DYNLT1-interacting proteins are indeed in an exposed protein surface and whether these proteins do, in fact, bind to DYNLT1. We describe below how
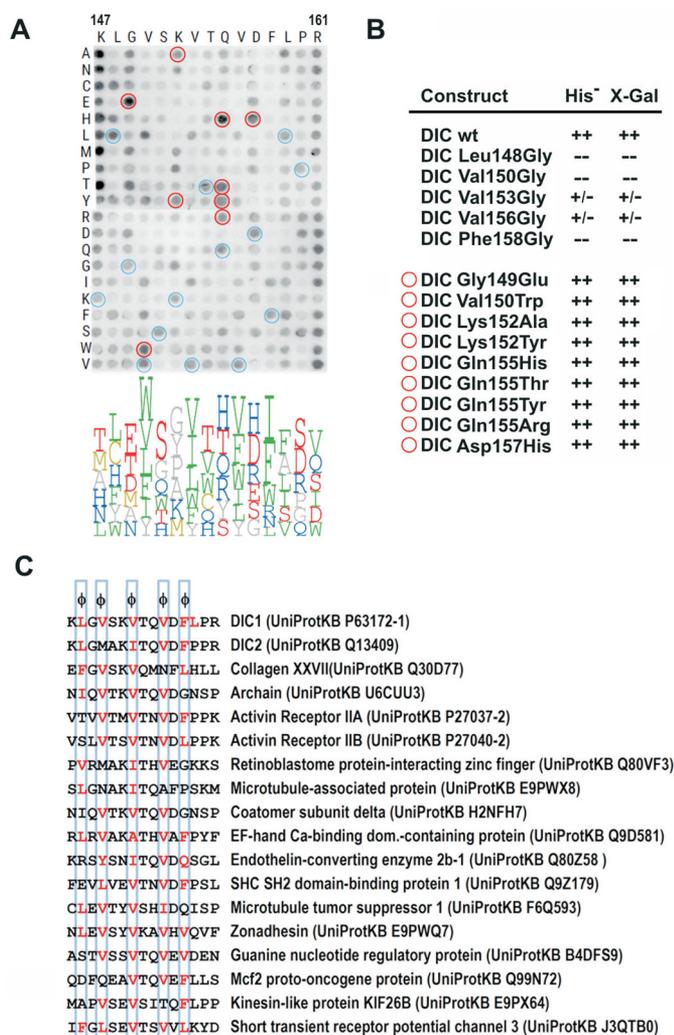
FIGURE 4. **Analysis of the binding plasticity of DYNLT1 canonical groove.** *A*, binding of DYNLT1 to a matrix of pentadecapeptides corresponding to human dynein intermediate chain in which each position was substituted by every natural amino acid. Recombinant DYNLT1 was incubated with a cellulose membrane bearing 300 spots with synthetic pentadecapeptides that expand the binding possibilities. The membrane was developed by ECL after incubation with an anti-DYNLT1 antibody followed by a secondary peroxidase-labeled antibody. A logo distribution is shown at the *bottom* obtained after densitometric quantification of the spots. Only the six residues with higher signal are shown for clarity. Residues below average signal were not included in the logo representation. *Blue circles* indicate identical substitutions that serve as positive controls. *Red circles* indicate substitutions that rendered positive binding and were subsequently confirmed in the yeast two-hybrid assay. *B*, yeast two-hybrid assay using DYNLT1 in the bait plasmid and various dynein intermediate chain constructs. Growth in the absence of the amino acid His and presence of 3-aminotriazole and X-Gal activity are shown. The *upper* part shows the binding assay for constructs in which hydrophobic amino acids have been mutated into Gly (L148G, V150G, V153G, V156G, and F158G). The *bottom* part shows dynein intermediate chain mutants with increased binding to DYNLT1 in the pepscan experiment. In several cases, these mutations comprise non-conservative substitutions and are hence difficult to predict. *C*, list of proposed cellular DYNLT1-interacting partners according to the results obtained in the pepscan analysis.

DYNLT1 interacts with one of these proteins targets, activin receptor IIB.

DYNLT1 Interacts with the Intracellular Domain of Activin Receptor IIB—In cells, a significant part of DYNLT1 is not attached to the dynein complex (29), raising the possibility that DYNLT1 might play roles unrelated to retrograde microtu-

bule-associated movement. The homodimeric structure of DYNLT1 and the positioning of the interacting partners within the canonical binding grooves indicate that DYNLT1 might function as a dimerization clamp in a similar fashion as that described for DYNLL1 (12). Among the proposed DYNLT1-associated proteins, we selected activin receptor II as a likely candidate to associate to DYNLT1. Activin receptor type IIB (ActRIIB) is a type II member of the family of serine/threonine kinase receptors that bind and are activated by the activin and myostatin signaling pathways (30). The N-terminal, extracellular part of ActRIIB binds to activin, whereas the C-terminal, intracellular part displays the serine/threonine kinase domain. We identified a potential DYNLT1 binding motif exactly at the very C-terminal end of ActRIIB with a sequence very similar to that shown by DIC (Fig. 5*A*). We confirmed in a yeast two-hybrid assay that a stretch comprising residues 428–512 of ActRIIB associates to DYNLT1 *in vitro*, hence establishing that both proteins do interact. Next, we created an ActRIIB construct in which the final 22 residues were deleted, resulting in a polypeptide that was unable to associate to DYNLT1. HEK293 cells were transfected with a C-terminally GFP-tagged full-length ActRIIB (residues 1–512) or GFP-tagged ActRIIB-ΔCt (residues 1–490). Confocal microscopy studies revealed that both full-length and the C-terminally deleted ActRIIB constructs localized to the plasma membrane and endomembranes. In contrast, as expected (16, 29), an mCherry-tagged DYNLT1 displayed a nuclear and cytosolic staining that extended essentially throughout the entire cell (Fig. 5*B*). Hence, because of the essentially identical subcellular distribution of full-length ActRIIB when compared with its GFP-tagged ActRIIB-ΔCt counterpart, we were unable to determine whether the association of ActRIIB and DYNLT1 took place at the plasma membrane or in intracellular membranes during the sorting pathway. Nevertheless, DYNLT1 associated to full-length ActRIIB but not to its ActRIIB-ΔCt counterpart when transfected in COS7 cells (Fig. 5*C*), hence reinforcing the notion that they associate in cells. We next investigated whether DYNLT1 was also involved in the signaling pathway of TGF-β using a luciferase reporter assay. Overexpression of both full-length ActRIIB and ActRIIB-ΔCt in the presence of the p3TP-lux plasmid in transfected HEK293 cells resulted in a significant increase of the reporter activity (Fig. 5*D*). Interestingly, deletion of the DYNLT1 binding site in the context of a functional ActRIIB resulted in a marked increase of the reporter activity. Likewise, overexpression of a FLAG-tagged DYNLT1 construct that could bind to transfected full-length ActRIIB resulted in a diminished signaling response. Taken together, our data indicate that DYNLT1 binding to ActRIIB results in the inhibition of its signaling activity.

The Binding Site of Lfc within DYNLT1 Extends Well Beyond the Canonical Binding Groove—The association between DYNLT1 and guanine nucleotide exchange factor Lfc has been analyzed extensively (15, 27, 31). Interestingly, it has been reported that Lfc associates within the DYNLT1 canonical binding groove and, at the same time, seems to be transported along microtubules, two observations that seem contradictory. Sequence comparison between DIC and Lfc reveals that the latter essentially maintains the five hydrophobic residues
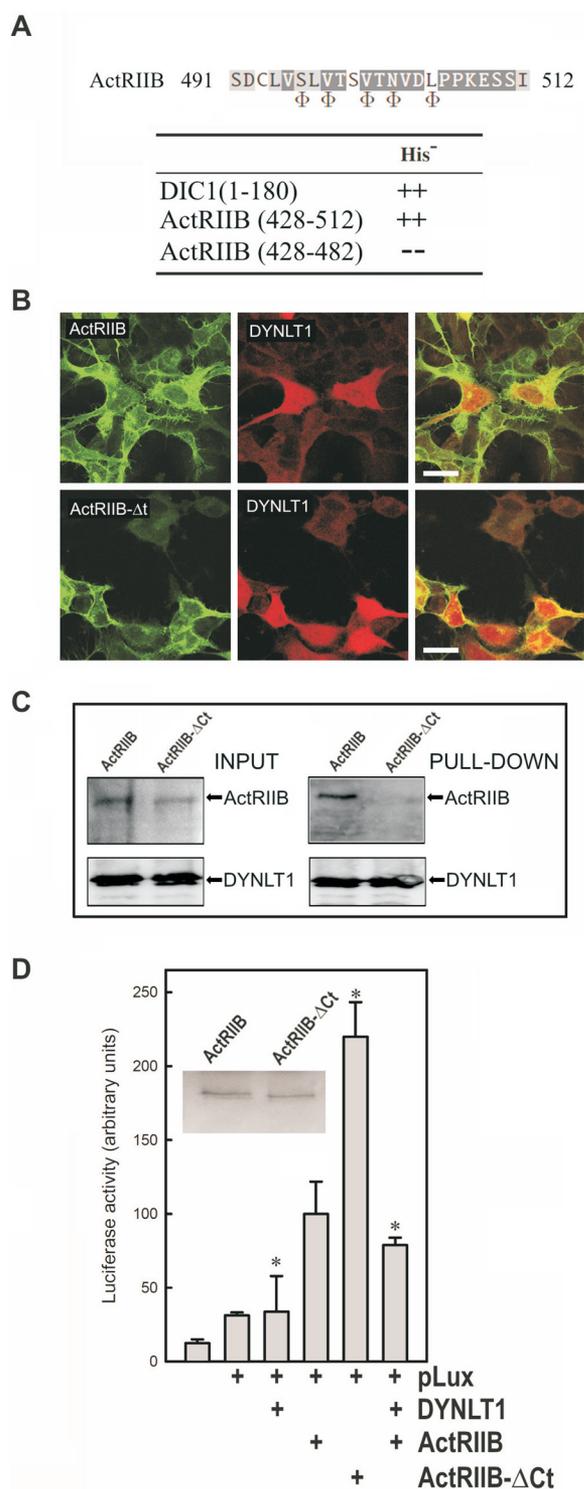
A

ActRIIB 491 SDCLVSLVTSVTNVDLPPKESSI 512

	His⁻
DIC1(1-180)	++
ActRIIB (428-512)	++
ActRIIB (428-482)	--

B

C

D

FIGURE 5. **Binding of DYNLT1 to the intracellular C terminus of activin receptor IIB inhibits its signaling properties.** *A*, sequence of ActRIIB at the binding site within the canonical groove of DYNLT1. The positions where hydrophobic amino acids are expected are shown at the bottom using the Φ symbol. Interaction between the C terminus of ActRIIB(428–512) and DYNLT1 in a yeast two-hybrid assay is shown. DIC1 was included as a positive control. *B*, confocal microscopy immunofluorescence of HEK293 cells transfected with mCherry-tagged DYNLT1 together with GFP-tagged ActRIIB constructs. The *upper panels* show full-length GFP-tagged ActRIIB, whereas the *bottom panels* show C-terminally deleted GFP-tagged ActRIIB. Merged panels are shown to the *right* in both cases. *Scale bars*, 25 μm. *C*, lectin-tagged DYNLT1 and full-length ActRIIB or its ActRIIB-ΔCt counterpart in transfected COS7 cells were allowed to associate, and the DYNLT1 moiety was sedimented with Sepharose beads. The appearance of each protein in the pellet fraction was

known to fit within the canonical binding groove, but, surprisingly, various residues seem to be conserved upstream of this canonical binding stretch (Fig. 6*A*). Remarkably, upstream from the predicted stretch that would insert within the hydrophobic binding groove of DYNLT1, Lfc also displayed a polybasic motif. Using a yeast two-hybrid assay, we tried to identify the minimal DYNLT1 binding region of Lfc. If Lfc could behave in the same manner as DIC, a 20-amino acid stretch comprising Lfc residues 142–161 (SSL . . . FND) would be enough to render a positive interaction with DYNLT1. In contrast, not even an Lfc construct comprising residues 135–180 could result in a detectable binding to DYNLT1 (Fig. 6*B*). In agreement with previously published results (31), we concluded that only large portions of Lfc could interact with DYNLT1. The most likely explanation for this piece of data would be that the Lfc-DYNLT1 interaction requires additional contacts involving residues lying outside the canonical binding groove. It is tempting to speculate that the N-terminal part of Lfc, lying outside the hydrophobic groove, might interact with the α-helices of DYNLT1 as proposed previously (15). It must be mentioned, in this context, that DIC itself displays both a polybasic stretch and the PS and QS motifs found in Lfc (Fig. 6*A*). This may indicate that even DIC might have secondary binding sites to the surface of DYNLT1 that were identified neither in the crystal structures of the DIC-DYNLT1 complexes nor in our NMR solution structure (see below). To further prove that Lfc binding to DYNLT1 requires extensive contacts lying outside the consensus binding groove, we used ITC and tested two long peptides of Lfc. Using ITC, we could detect the binding of both Lfc(131–154) or Lfc(131–161) peptides to DYNLT1. The longer peptide rendered a K_d of 11.7 ± 0.9 μM (thermodynamic parameters: $\Delta G = -6.72$ kcal/mol, $\Delta H = -4.03$ kcal/mol, and $-T\Delta S = 2.70$ kcal/mol), whereas the shorter peptide rendered a K_d of 78 ± 1.5 μM (thermodynamic parameters: $\Delta G = -5.59$ kcal/mol, $\Delta H = -9.05$ kcal/mol, and $-T\Delta S = 3.46$ kcal/mol). Further confirmation of the extended DYNLT1 binding site within Lfc was obtained when a shorter peptide corresponding to Lfc(137–154) showed no binding heat in an ITC assay (Fig. 6*C*).

Next, to assess whether the polybasic residues present in Lfc preceding the part predicted to insert within the canonical groove are involved in the interaction, we mutated Arg[138]/Arg[139] and confirmed that the mutant Lfc polypeptide showed a significant lowered interaction in a yeast two-hybrid assay (Fig. 6*D*). Likewise, an Lfc G140A mutant bound poorly to DYNLT1. Somehow expectedly, mutant Lfc constructs of residues known to insert in the hydrophobic groove (Val[150], Ser[151], and Thr[153]) completely failed to interact with DYNLT1.

It has been shown previously that binding of microtubules to Lfc and to its homolog GEF-H1 might be regulated through Ser phosphorylation. For instance, polarity kinase Par1b phosphor-

determined with the appropriate antibodies. *D*, the effect of DYNLT1 on ActRIIB signaling was analyzed in transfected HEK293 cells using a luciferase reporter construct. The *inset* shows a Western blot of transfected ActRIIB and ActRIIB-ΔCt. All experiments were performed in duplicate wells and repeated three times. The results show average -fold changes and refer to transfected wild-type ActRIIB in the presence of p3TP-lux plasmid. S.D. values are indicated by *error bars* with * indicating $p < 0.05$.
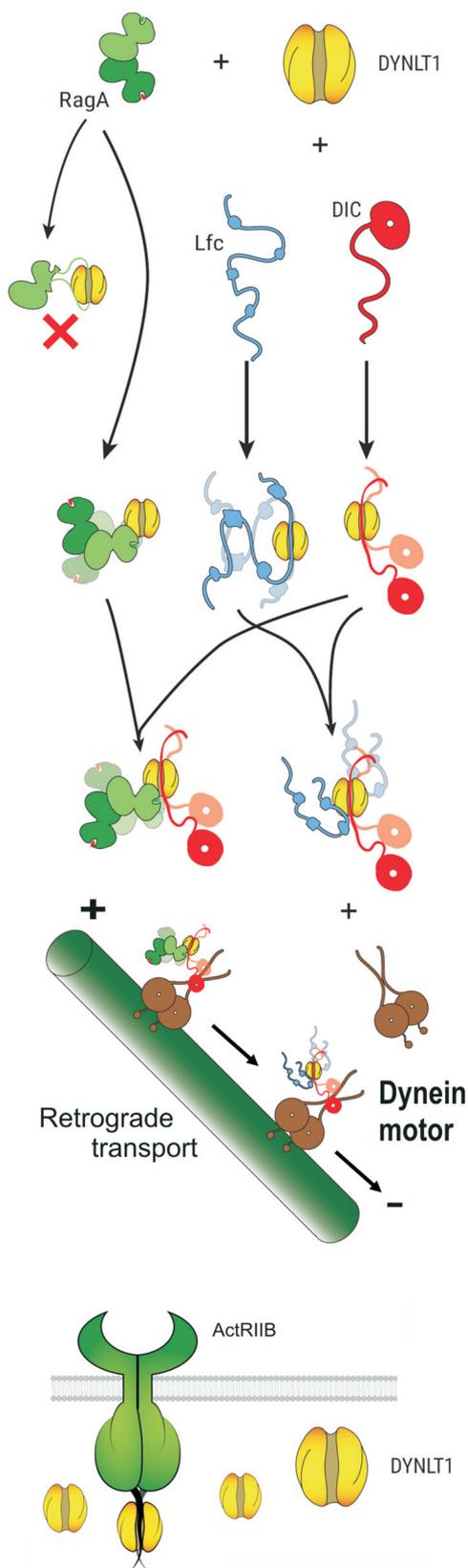
FIGURE 6. **Characterization of DYNLT1 binding to guanine nucleotide exchange factor Lfc.** *A*, sequence comparison between DIC and Lfc. The binding region to DYNLT1 and DYNLL1 is shown. The positions where hydrophobic amino acids are expected are marked at the *bottom line* using the symbol Φ. *B*, yeast-two hybrid assay in which DYNLT1 was confronted to various DIC and Lfc constructs. Growth in the absence of the amino acid His and presence of 3-aminotriazole and X-Gal activity are shown. *C*, ITC analysis of the binding of peptides Lfc(131–161), Lfc(131–154), and Lfc(137–154) to purified DYNLT1. The thermogram is shown in the *upper panel*, and the binding isotherm is shown in the *bottom panel*. Curve fitting rendered K_d values of 11.7 ± 0.9 μM for Lfc(131–161) and 78 ± 1.5 μM for Lfc(131–154). Peptide Lfc(137–154) gave no binding heat. *D*, yeast-two hybrid assay in which DYNLT1 was confronted to various Lfc constructs. Growth in the absence of the amino acid His and presence of 3-aminotriazole and X-Gal activity are shown. *E*, representative binding curve for a FITC-labeled DIC1 peptide (amino acids 118–178) to DYNLT1 measured by fluorescence polarization. A calculated K_d of 1.56 ± 0.8 μM could be obtained. Results are representative of three independent experiments. *F*, sequence comparison between six DYNLT1-binding partners showing the position of the stretch that inserts within the hydrophobic binding groove (in *blue*) and the basic residues (in *red*). The polybasic region is shown on *top*. Please note that the Ser-Ser motif present in Lfc and parathyroid hormone-related protein receptor (*PTHR*) probably becomes phosphorylated *in vivo*. *mP*, millipolarization units.

ylates GEF-H1 Ser[143] (32), a post-translational modification proposed to disrupt its interaction to DYNLT1 and to release it from the dynein motor (15). In fact, analysis of the Lfc stretch [138]RRGRSS[143] using kinase phosphorylation prediction programs easily reveals that both Ser[142] and Ser[143] could be substrates of several other protein kinases such as ATM, GSK-3, or AKT1. Hence, the presence of these two phosphorylatable Ser residues within the DYNLT1 binding stretch of Lfc might be a way of regulating this interaction.

To determine whether DIC1 residues N-terminal to those known to become inserted within the binding groove might also contribute to the overall binding energy, we tested the binding of a longer FITC-labeled DIC1 fragment (residues 118–178) using fluorescence polarization measurements. The

K_d value between probe and DYNLT1 was determined to be 1.56 ± 0.8 μM (Fig. 6*E*). Hence, both the PS and QS motifs of DIC1 or other upstream residues contribute to the association to DYNLT1 because we previously obtained a K_d value of 4.80 ± 0.5 μM when using the FITC-labeled DIC1(147–162) peptide (Fig. 1*E*).

Other DYNLT1-interacting Partners Might Adopt a Similar Way of Interaction—Sequence comparison of DIC, ActRIIB, and Lfc with other proteins known to bind to DYNLT1 such as the parathyroid hormone-related protein receptor (33), poliovirus receptor CD155 (34), and the neuronal protein Doc2 (20) reveals a similar amino acid distribution (Fig. 6*F*). In general, these proteins do have hydrophobic amino acids at the five positions where residues are expected to fulfill this require-

FIGURE 7. **Proposed interaction model of DYNLT1 with various character-ized targets.** The small GTPases RagA and Rab3D (labeled *green*) bind to the surface of DYNLT1 and do not occupy the canonical binding groove. Hence, DYNLT1 functions as a dimerization clamp that subsequently links these proteins to DIC (labeled *red*) and finally to the dynein motor. Conversely, Lfc (labeled in *blue*) can occupy the canonical binding groove and part of the surface of DYNLT1. Because it is clearly established that DYNLT1 connects Lfc and its homolog

ment. In most cases, the sequence known to insert within the canonical binding groove is preceded by a stretch of basic amino acids. Furthermore, parathyroid hormone protein receptor displays phosphorylatable Ser residues immediately following these basic residues, suggesting that phosphorylation might also regulate its binding to DYNLT1.

Discussion

Microtubules are hollow cylindrical fibers of ~25 nm in diameter that are formed by the polymerization of the α,β-tubulin heterodimer. Organelles, vesicles, and other intracellular cargoes are transported by kinesin and dynein motors, which move in opposite directions along microtubules. In the case of the dynein motor, the identity of the precise dynein polypeptides involved in cargo binding remains the subject of much debate. Dynein light chains DYNLL (DLC8) and DYNLT (Tctex) have been proposed as cargo adaptors because of their ability to bind to DIC and their ability to bind to multiple cellular and viral proteins. We have recently shown that the small GTPases RagA and Rab3D are *bona fide* DYNLT1-interacting proteins that associate to this dynein light chain when forming part of the dynein motor (16). However, among the over 20 DYNLT1-binding proteins, it is not well established which ones use the canonical binding groove and which ones bind to the surface of DYNLT1.

Our data also suggest that not only Lfc, but also DIC itself, very likely establish contacts with DYNLT1 in superficial areas distant from the hydrophobic groove. However, in the case of DIC, a short stretch inserting in the groove renders a positive interaction, whereas in the case of Lfc both contact areas seem to be necessary for binding. Furthermore, unlike DIC when binding to DYNLT1, the lower affinity association of Lfc to DYNLT1 is very likely regulated through Lfc Ser phosphorylation.

We also describe herein the interaction between DYNLT1/Tctex1 and activin receptor IIB. Interestingly, Tctex2β, another dynein light chain family isoform, binds to several members of the transforming growth factor-β receptors, such as endoglin TβRII, betaglycan, and ActRIIA (35). Tctex2β has two clearly defined domains and is larger than DYNLT1/Tctex1 although not so dissimilar because its C-terminal part is highly homologous to DYNLT1/Tctex1. In agreement with our results, overexpression of Tctex2β also inhibits TGF-β signaling. Likewise, there is a significant colocalization of endoglin and Tctex2β in endomembranes when cotransfected in HEK293 cells. The suggestion that Tctex2β might bridge together endoglin and TβRII (35) raises the possibility of DYNLT1/Tctex1 also forming part of tripartite complexes with transmembrane TGF-β receptors and hence regulating their activity. Further studies will be necessary to address this issue.

With all the available data, we can propose different modes of protein binding to dynein light chain DYNLT1 (Fig. 7). Small

GEF-H1 to microtubules (15, 31, 32), binding of DIC would displace Lfc from the binding groove without dissociating the trimeric complex. These guanine nucleotide exchange factors must remain associated to DYNLT1 and become attached to the dynein motor and to microtubules. Finally, ActRIIB and other TGF-β receptors use DYNLT1 (or perhaps its homolog Tctex2β (35)) as molecular clamps to anchor their C termini. It is not known whether DYNLT1 can also mediate heterodimerization of different TGF-β receptors.

Canonical Binding Site of DYNLT1

GTPases such as RagA can bind to the surface of both DYNLT1 and DYNLT1-DIC2 efficiently (16), subsequently forming a tripartite complex with DIC and becoming attached to microtubules via the dynein motor. Conversely, Lfc and its homolog GEF-H1 bind to DYNLT1 using two sites, but eventually the canonical binding groove becomes occupied by DIC itself, allowing the formation of a tripartite complex (15) that can be subsequently targeted to microtubules via the dynein motor. Because it is very well established that both small GTPases of the RagA and Rab3D families as well as the guanine nucleotide exchange factors Lfc and GEF-H1 do associate to microtubules (15, 16, 32, 36), the formation of a tripartite complex involving DIC-DYNLT1-protein must take place. Conversely, a significant population of DYNLT1 is not attached to microtubules (29), most likely being involved in functioning as a molecular dimerization clamp of cytoplasmic proteins. We propose (Fig. 7, *bottom* part) that DYNLT1 functions as a dimerization clamp for the TGF-β family receptor ActRIIB in an association not involving the subsequent attachment to microtubules.

Although other cargo adapters beyond DYNLT1 have been reported such as intermediate chain itself upon binding to circovirus proteins (37) or the Hsp90-immunophilin complex that is associated to dynactin necessary for p53 binding (38), our data put forward novel ways of cargo attachment through DYNLT1. In summary, our results shed light on the binding mechanism of DYNLT1 to various protein targets, describe the solution structure of the first mammalian DYNLT1 isoform, and rationalize under which circumstances targeting to microtubules of the attached protein occurs.

Experimental Procedures

Materials—^{15}N-Labeled NH_4Cl and ^{13}C-labeled glucose were purchased from Cambridge Isotope Laboratories. Buffers, chemicals, oligonucleotides, and common laboratory reagents were obtained from Sigma-Aldrich if not otherwise indicated. *Pfu* polymerase, T4 DNA ligase, restriction endonucleases, and molecular mass markers were obtained from Fermentas. Synthetic peptides were ordered from Thermo Scientific and were at least 90% pure. Sepharose 4B was from GE Healthcare. D(+)-Lactose monohydrate was from Scharlau. Glutamine, antibiotics, cell culture medium (Dulbecco's modified Eagle's medium) and X-Gal (5-bromo-4-chloro-3-indolyl β-D-galactoside) were purchased from Sigma-Aldrich. Trypsin-EDTA and fetal bovine serum were from BioWhittaker Europe.

Constructs—The mouse DYNLT1 cDNA (UniProtKB P51807), kindly provided by Dr. Thomas Sakmar (The Rockefeller University, New York) (19), was amplified and cloned into the yeast two-hybrid vectors pGAD and pGBT9 as well as into the recombinant expression vector pKLSLt (39). Mammalian expression vectors were also created using the LSLt lectin (39) in-frame with DYNLT1 or DYNLT1-DIC2 (16). The human DYNLT1 cDNA (UniProtKB P63172) was a generous gift from Dr. Laszlo Nyitray (Eötvös Loránd University, Budapest), provided in the recombinant expression vector pBH4 with a His$_6$ tag and a tobacco etch virus protease cleavage sequence. The full-length mouse dynein intermediate chain DYNC1I2 (UniProtKB O88485) was provided by Dr. Mingjie Zhang (The Hong Kong University of Science and Technology) (7). The

sequence of DIC known to bind to DYNLT1 and DYNLL1 (amino acids 130–160) was amplified and cloned in the yeast two-hybrid and recombinant expression vectors as described above. The self-saturated DYNLT1-DIC2 chimeric protein was created by fusing the DYNLT1 binding region of the human DIC2 (UniProt Q13409) to the C terminus of human DYNLT1 in-frame after a short linker. The sequence of the resulting fusion protein is shown in Figure 2*A*. DYNLT1-DIC2 was cloned into the pBH4 vector for recombinant expression (16). Mouse activin receptor IIB (UniProtKB P27040–2) and p3TP-lux (a reporter of TGF-β signaling) plasmids were provided by Dr. Carmelo Bernabeu (Centro de Investigaciones Biológicas, Madrid, Spain). The C-terminal deletion construct of ActRIIB was obtained by PCR and included residues 1–490, whereas full-length wild-type ActRIIB was 512 amino acids long. We also obtained GFP-tagged constructs of both full-length and ActRIIB-ΔCt using a commercial pEGFP-N vector. Full-length Lfc cDNA (UniProtKB Q865S3) was a kind gift from Dr. Karl Matter (University College London, London, UK).

Yeast Two-hybrid and β-Galactosidase Assay—We used plasmids containing the GAL4 binding domain that were confronted with plasmids containing the GAL4 activation domain as described previously (40, 41). Double transformants were plated in Leu$^-$/Trp$^-$/His$^-$ synthetic defined plates in the presence of 12 mM 3-aminotriazole (triple dropout plates) as well as in Leu$^-$/Trp$^-$/His$^+$. Interacting proteins expressed within the same yeast resulted in colonies that could rescue growth in the absence of His. These colonies were subsequently screened in the X-Gal assay. Blue colonies corresponded to a positive interaction, whereas white colonies corresponded to absence of interaction.

Recombinant Protein Expression and Purification—The pBH4-DYNLT1 and pBH4-DYNLT1-DIC2 plasmids were used to transform BL21 DE3 *Escherichia coli*. 2 liters of bacterial culture in 2× yeast extract-tryptone were routinely used for recombinant expression. When the protein was used for NMR experiments, the bacteria transformed with pBH4-DYNLT1 were grown in M9 minimal medium supplemented with ^{15}N-labeled NH_4Cl or ^{15}N-labeled NH_4Cl plus ^{13}C-labeled glucose. Protein expression was induced by addition of 0.5 mM isopropyl 1-thio-β-D-galactopyranoside and incubation overnight at 20 °C with 150 rpm aeration rate. Bacterial cells were pelleted and frozen at -20 °C until used for protein purification.

Briefly, the bacterial cell lysis was performed on ice in lysis buffer (50 mM NaH_2PO_4, 300 mM NaCl, 3 mM NaN_3, pH 8) with continuous stirring in the presence of protease inhibitors (1 μg/ml aprotinin, 1 μg/ml leupeptin, and 200 μM PMSF), 200 mg/liter lysozyme, and 5 mM β-mercaptoethanol followed by four cycles of sonication on ice. The cell lysate was clarified by centrifugation at 10,000 × g and filtered through porous paper. The recombinant His$_6$-tagged proteins were sequentially purified using a nickel-nitrilotriacetic acid affinity column followed by a digestion with tobacco etch virus protease and a final separation using a HiTRAP Q HP anionic exchange column. The protein purity was confirmed by SDS-PAGE and Coomassie Blue staining. Pure protein solutions were concentrated by centrifugation in Centricon® tubes (Millipore) to a final concentration of ~1 mM. When DYNLT1 was expressed in mammalian

cells, the vector pKLSLt-DYNLT1 was used to transform COS7 cells. Protein purification was performed 36 h post-transfection using the protocol described above. DYNLT1 expressed in mammalian cells was used in the pepscan assays.

ITC—The interaction between DYNLT1 and the various peptides was measured using a VP-ITC MicroCalorimeter (MicroCal, Northampton, MA) in 20 mM Hepes buffer, pH 7.4, containing 0.15 M NaCl at 25 °C as reported previously (42). Commercial peptides were dissolved in water at a 2 mM concentration and subsequently diluted to 0.5–1 mM in the aforementioned buffer when put in the syringe. The protein solutions were introduced into the sample cells, whereas the peptides were in the syringe. All samples were degassed for at least 5 min in a ThermoVac (MicroCal). Control experiments were performed whereby peptides were titrated into buffer and buffer-titrated into DYNLT1. As a rule, each experiment consisted of an initial injection of 2.5 μl followed by 30 7.5-μl injections. The heat released in each injection was calculated from the raw data by integration of the peaks after subtraction of the baseline. All data were analyzed using the Origin®5 program.

Cell Transfection and Immunofluorescence—We followed the procedures described previously by our group (41, 43). COS7 cells were from the European Collection of Cell Cultures.

Fluorescence Polarization Assays—Fluorescence polarization (FP) was performed in a PerkinElmer Life Sciences MPF 44-E spectrofluorometer. Saturation binding experiments were performed for measuring binding affinity (K_d) between FITC-labeled peptides and DYNLT1 by applying an increasing amount of recombinant protein (typically 0–150 μM) to a fixed and low concentration of probe (5–100 nM). Incubation time was 10–15 min (room temperature), and the assay was performed in 20 mM Hepes, 150 mM NaCl, pH 7.4, in a final volume of 0.5 ml. Polarization of the FITC-labeled peptides was measured at excitation/emission values of 488/530 nm (bandwidth, 10 nm). The fluorescence anisotropy (r) values were obtained using the fluorescence polarization (P) values with the equation $r = 2P/(3 - P)$. The initial anisotropy (r_i) in the absence of added protein was measured. The FP values were fitted to the equation $(FP - FP_0) = (FP_{max} - FP_0)[PDZ domain]/(K_d + [PDZ domain])$ where FP is the measured fluorescence polarization, FP_{max} is the maximal fluorescence polarization value, FP_0 is the fluorescence polarization in the absence of added PDZ domain, and K_d is the dissociation constant. As long as the concentration of labeled peptide is well below the true K_d during the assay, the K_d can be directly derived from this saturation curve.

NMR Experiments—Pure unlabeled, ^{15}N-labeled, and doubly ^{13}C,[15]N-labeled human DYNLT-DIC in the range of 50–200 μM was prepared in water with 10% D_2O in 100 mM KH_2PO_4 buffer, 1 mM DTT, pH 7.0. NMR samples contained 50 μM sodium 2,2-dimethyl-2-silapentane-5-sulfonate as an internal reference.

NMR spectra were acquired at 298 K on a Bruker AV 800 NMR spectrometer (Bruker, Rheinstetten, Germany) equipped with a triple resonance z-gradient cryoprobe. [15]N and ^{13}C chemical shifts were referenced indirectly using the gyromagnetic ratios of [15]N:[1]H and [13]C:[1]H (44). The following standard pulse sequences, corresponding to the heteronuclear multidimensional approach for NMR assignments (45), were acquired

and analyzed: 2D [1]H-^{1}H NOESY (80 ms), ^{15}N HSQC, and ^{13}C HSQC and 3D spectra CBCA(CO)NH, CBCANH, HNCA, HN(CO)CA, HC(C)H TOCSY, (H)CCH TOCSY, ^{1}H-^{15}N HSQC-NOESY (50 ms), ^{1}H-^{13}C HSQC-NOESY (50 ms, aliphatic region), and ^{1}H-^{13}C HSQC-NOESY (50 ms, aromatic region).

The spectra were processed with Bruker Topspin 2.1 (Bruker, Germany), and spectral analysis was performed with Sparky 3 (46). Backbone and side chain ^{1}H, ^{13}C, and ^{15}N chemical shifts were assigned following conventional strategies. The resonance list is nearly complete and has been deposited in the BioMagResBank under the code number 30074.

Structure Calculation—The structure calculation of the DYNLT-DIC construct was performed with CYANA (47) using the symmetric homodimer protocol and the automatic NOE assignment facility combined with lists of manually assigned NOEs. In total, there were 3247 upper distance constraints, 143 of which were manually assigned. 514 backbone dihedral angle constraints were determined from chemical shift values using TALOS+ (48). Initially, 100 conformers were generated that were forced to satisfy experimental data using a standard automatic CYANA protocol. The 20 conformers with the lowest final CYANA target function values were selected for further refinement and finally minimized with Amber9 software (49) using the Gibbs-Boltzmann continuum solvation model. Final structure quality was checked with PROCHECK-NMR (50), and the coordinates have been deposited in the Protein Data Bank under the accession number 5JPW. MOLMOL (51) and PyMOL (Schrödinger, LLC) were used for molecular analysis and display.

NMR Dynamics—[1]H-^{15}N heteronuclear NOE data were determined on the bases of conventional NOE measurements with a ^{15}N-labeled sample. Experiments with and without proton saturation were acquired simultaneously in an interleaved manner with a recycling delay of 10 s and split during processing into separate spectra for analysis. The values for the heteronuclear NOEs were obtained from the ratio intensities of the resonances according to I_{sat}/I_{ref}. Intensities and peak volumes were determined by using tools included in Sparky (46). The uncertainty was estimated to be about 5%.

Circular Dichroism Measurements—CD spectra were recorded on a Jasco J-715 spectropolarimeter using a 0.1-cm-path length cell for the far-UV measurements at 25 °C as reported previously (52). Data analysis was performed using Microcal Origin software (Originlab, Northampton, MA).

Luciferase Reporter Assay—Luciferase activity was measured using the Dual-Glo® Luciferase Assay System kit (Promega, Madison, WI) as specified by the manufacturer in an EG&G Berthold Lumat LB 9507 luminometer. Briefly, HEK cells were transfected with the p3TP-lux plasmid in the presence or absence of full-length ActRIIB or an ActRIIB lacking the DYNLT1 binding site present at its cytoplasmic C terminus (referred to as ActRIIB-ΔCt). Subsequently, cells were washed once with phosphate-buffered saline. After addition of 200 μl of lysis buffer, cells were scraped and centrifuged (4 °C, 12,000 × g, 5 min). Measurement was carried out in 1:1 dilutions of the cell extract with the Dual-Glo Luciferase Reagent followed by

an incubation of 10 min within 2 h. Each sample was measured for 20 s. All assays were performed in duplicate.

Cell Transfection and Pulldown Assays—We followed the procedures described previously by our group (16, 42). The association between LSLt-DYNLT1 and either GFP-tagged full-length ActRIIB-GFP (residues 1–512) or GFP-tagged ActRIIB-ΔCt (residues 1–490) in transfected COS7 cells was analyzed. The pulldown assays were performed using Sepharose 4B in the absence of added antibodies. The cell extract was incubated with protease inhibitors plus alkaline phosphatase and clarified, and the radioimmune precipitation assay buffer-solubilized proteins were allowed to bind to Sepharose 4B beads due to the presence of the LSLt lectin. The beads were subsequently extensively washed to avoid nonspecific interactions of the cellular extract and processed as in a conventional immunoprecipitation.

Pepscan Experiments—Automated peptide spot synthesis attached to a cellulose membrane (Abimed, Langenfeld, Germany) and incubation with the desired recombinant protein was performed using the pepscan methodology as reported previously (53, 54). The membrane was obtained with the synthesized pentadecapeptides immobilized by their C termini via a polyethylene glycol spacer and N-terminally acetylated. The cellulose membranes were coated with 1% nonfat dried milk in TBS (50 mM Tris, pH 7.0, 137 mM NaCl, 2.7 mM KCl) for 4 h at room temperature. Incubation with the recombinant DYNLT1 (0.1 μM) was done overnight at room temperature. Three washes (25 ml each) were performed with TBS, 0.05% Tween 20. Subsequently, the membrane was incubated for 2 h at room temperature with an antibody against DYNLT1. Three additional 10-min washes were performed with TBS, 0.05% Tween 20 followed by three more 10-min washes with TBS alone. Development of the membrane was performed by ECL following the manufacturer's instructions. The intensity of each spot was subsequently quantified using Fuji software.

Author Contributions—J. M.-G., H. Z.-C., M. B., and I. R.-C. designed and performed the experiments. M. B. and I. R.-C. wrote the manuscript.

References

1. King, S. M. (2000) The dynein microtubule motor. *Biochim. Biophys. Acta* **1496,** 60–75
2. Allan, V. J. (2011) Cytoplasmic dynein. *Biochem. Soc. Trans.* **39,** 1169–1178
3. Pfister, K. K., Shah, P. R., Hummerich, H., Russ, A., Cotton, J., Annuar, A. A., King, S. M., and Fisher, E. M. (2006) Genetic analysis of the cytoplasmic dynein subunit families. *PLoS Genet.* **2,** e1
4. Pfister, K. K., Fisher, E. M., Gibbons, I. R., Hays, T. S., Holzbaur, E. L., McIntosh, J. R., Porter, M. E., Schroer, T. A., Vaughan, K. T., Witman, G. B., King, S. M., and Vallee, R. B. (2005) Cytoplasmic dynein nomenclature. *J. Cell Biol.* **171,** 411–413
5. Wu, H., Maciejewski, M. W., Takebe, S., and King, S. M. (2005) Solution structure of the Tctex1 dimer reveals a mechanism for dynein-cargo interactions. *Structure* **13,** 213–223
6. Wu, H., Maciejewski, M. W., Marintchev, A., Benashski, S. E., Mullen, G. P., and King, S. M. (2000) Solution structure of a dynein motor domain associated light chain. *Nat. Struct. Biol.* **7,** 575–579
7. Fan, J., Zhang, Q., Tochio, H., Li, M., and Zhang, M. (2001) Structural basis of diverse sequence-dependent target recognition by the 8 kDa dynein light chain. *J. Mol. Biol.* **306,** 97–108
8. Rapali, P., Szenes, Á., Radnai, L., Bakos, A., Pál, G., and Nyitray, L. (2011) DYNLL/LC8: a light chain subunit of the dynein motor complex and beyond. *FEBS J.* **278,** 2980–2996
9. Hall, J., Karplus, P. A., and Barbar, E. (2009) Multivalency in the assembly of intrinsically disordered dynein intermediate chain. *J. Biol. Chem.* **284,** 33115–33121
10. Williams, J. C., Roulhac, P. L., Roy, A. G., Vallee, R. B., Fitzgerald, M. C., and Hendrickson, W. A. (2007) Structural and thermodynamic characterization of a cytoplasmic dynein light chain-intermediate chain complex. *Proc. Natl. Acad. Sci. U.S.A.* **104,** 10028–10033
11. Nyarko, A., and Barbar, E. (2011) Light chain-dependent self-association of dynein intermediate chain. *J. Biol. Chem.* **286,** 1556–1566
12. Barbar, E. (2008) Dynein light chain LC8 is a dimerization hub essential in diverse protein networks. *Biochemistry* **47,** 503–508
13. García-Mayoral, M. F., Rodríguez-Crespo, I., and Bruix, M. (2011) Structural models of DYNLL1 with interacting partners: African swine fever virus protein p54 and postsynaptic scaffolding protein gephyrin. *FEBS Lett.* **585,** 53–57
14. García-Mayoral, M. F., Martínez-Moreno, M., Albar, J. P., Rodríguez-Crespo, I., and Bruix, M. (2010) Structural basis for the interaction between dynein light chain 1 and the glutamate channel homolog GRINL1A. *FEBS J.* **277,** 2340–2350
15. Meiri, D., Marshall, C. B., Greeve, M. A., Kim, B., Balan, M., Suarez, F., Bakal, C., Wu, C., Larose, J., Fine, N., Ikura, M., and Rottapel, R. (2012) Mechanistic insight into the microtubule and actin cytoskeleton coupling through dynein-dependent RhoGEF inhibition. *Mol. Cell* **45,** 642–655
16. Merino-Gracia, J., García-Mayoral, M. F., Rapali, P., Valero, R. A., Bruix, M., and Rodríguez-Crespo, I. (2015) DYNLT (Tctex-1) forms a tripartite complex with dynein intermediate chain and RagA, hence linking this small GTPase to the dynein motor. *FEBS J.* **282,** 3945–3958
17. Williams, J. C., Siglin, A. E., Lightcap, C. M., and Amrita, D. (2012) Structural analysis of dynein intermediate and light chains, in *Dyneins: Structure Biology and Disease* (King, S. M., ed) pp. 157–189, Academic Press, New York
18. Merino-Gracia, J., García-Mayoral, M. F., and Rodríguez-Crespo, I. (2011) The association of viral proteins with host cell dynein components during virus infection. *FEBS J.* **278,** 2997–3011
19. Sachdev, P., Menon, S., Kastner, D. B., Chuang, J. Z., Yeh, T. Y., Conde, C., Caceres, A., Sung, C. H., and Sakmar, T. P. (2007) G protein βγ subunit interaction with the dynein light-chain component Tctex-1 regulates neurite outgrowth. *EMBO J.* **26,** 2621–2632
20. Nagano, F., Orita, S., Sasaki, T., Naito, A., Sakaguchi, G., Maeda, M., Watanabe, T., Kominami, E., Uchiyama, Y., and Takai, Y. (1998) Interaction of Doc2 with Tctex-1, a light chain of cytoplasmic dynein. Implication in dynein-dependent vesicle transport. *J. Biol. Chem.* **273,** 30065–30068
21. Bauch, A., Campbell, K. S., and Reth, M. (1998) Interaction of the CD5 cytoplasmic domain with the Ca^{2+}/calmodulin-dependent kinase IIδ. *Eur. J. Immunol.* **28,** 2167–2177
22. Mital, J., Lutter, E. I., Barger, A. C., Dooley, C. A., and Hackstadt, T. (2015) Chlamydia trachomatis inclusion membrane protein CT850 interacts with the dynein light chain DYNLT1 (Tctex1). *Biochem. Biophys. Res. Commun.* **462,** 165–170
23. Pfister, K. K., Salata, M. W., Dillman, J. F., 3rd, Vaughan, K. T., Vallee, R. B., Torre, E., and Lye, R. J. (1996) Differential expression and phosphorylation of the 74-kDa intermediate chains of cytoplasmic dynein in cultured neurons and glia. *J. Biol. Chem.* **271,** 1687–1694
24. Pfister, K. K., Salata, M. W., Dillman, J. F., 3rd, Torre, E., and Lye, R. J. (1996) Identification and developmental regulation of a neuron-specific subunit of cytoplasmic dynein. *Mol. Biol. Cell* **7,** 331–343
25. Mok, Y. K., Lo, K. W., and Zhang, M. (2001) Structure of Tctex-1 and its interaction with cytoplasmic dynein intermediate chain. *J. Biol. Chem.* **276,** 14067–14074

26. Makokha, M., Hare, M., Li, M., Hays, T., and Barbar, E. (2002) Interactions of cytoplasmic dynein light chains Tctex-1 and LC8 with the intermediate chain IC74. *Biochemistry* **41,** 4302–4311

27. Balan, M. (2013) *The Regulation of RhoGEF LFC by Dyenin Light Chain Tctex-1*. PhD Thesis, University of Toronto

28. Williams, J. C., Xie, H., and Hendrickson, W. A. (2005) Crystal structure of dynein light chain TcTex-1. *J. Biol. Chem.* **280,** 21981–21986

29. Tai, A. W., Chuang, J. Z., and Sung, C. H. (1998) Localization of Tctex-1, a cytoplasmic dynein light chain, to the Golgi apparatus and evidence for dynein complex heterogeneity. *J. Biol. Chem.* **273,** 19639–19649

30. Santibañez, J. F., Quintanilla, M., and Bernabeu, C. (2011) TGF-β/TGF-β receptor system and its role in physiological and pathological conditions. *Clin. Sci.* **121,** 233–251

31. Meiri, D., Marshall, C. B., Mokady, D., LaRose, J., Mullin, M., Gingras, A. C., Ikura, M., and Rottapel, R. (2014) Mechanistic insight into GPCR-mediated activation of the microtubule-associated RhoA exchange factor GEF-H1. *Nat. Commun.* **5,** 4857

32. Yoshimura, Y., and Miki, H. (2011) Dynamic regulation of GEF-H1 localization at microtubules by Par1b/MARK2. *Biochem. Biophys. Res. Commun.* **408,** 322–328

33. Sugai, M., Saito, M., Sukegawa, I., Katsushima, Y., Kinouchi, Y., Nakahata, N., Shimosegawa, T., Yanagisawa, T., and Sukegawa, J. (2003) PTH/PTH-related protein receptor interacts directly with Tctex-1 through its COOH terminus. *Biochem. Biophys. Res. Commun.* **311,** 24–31

34. Mueller, S., Cao, X., Welker, R., and Wimmer, E. (2002) Interaction of the poliovirus receptor CD155 with the dynein light chain Tctex-1 and its implication for poliovirus pathogenesis. *J. Biol. Chem.* **277,** 7897–7904

35. Meng, Q., Lux, A., Holloschi, A., Li, J., Hughes, J. M., Foerg, T., McCarthy, J. E., Heagerty, A. M., Kioschis, P., Hafner, M., and Garland, J. M. (2006) Identification of Tctex2β, a novel dynein light chain family member that interacts with different transforming growth factor-β receptors. *J. Biol. Chem.* **281,** 37069–37080

36. Pavlos, N. J., Cheng, T. S., Qin, A., Ng, P. Y., Feng, H. T., Ang, E. S., Carrello, A., Sung, C. H., Jahn, R., Zheng, M. H., and Xu, J. (2011) Tctex-1, a novel interaction partner of Rab3D, is required for osteoclastic bone resorption. *Mol. Cell. Biol.* **31,** 1551–1564

37. Cao, J., Lin, C., Wang, H., Wang, L., Zhou, N., Jin, Y., Liao, M., and Zhou, J. (2015) Circovirus transport proceeds via direct interaction of the cytoplasmic dynein IC1 subunit with the viral capsid protein. *J. Virol.* **89,** 2777–2791

38. Galigniana, M. D., Harrell, J. M., O'Hagen, H. M., Ljungman, M., and Pratt, W. B. (2004) Hsp90-binding immunophilins link p53 to dynein during p53 transport to the nucleus. *J. Biol. Chem.* **279,** 22483–22489

39. Angulo, I., Acebrón, I., de las Rivas, B., Muñoz, R., Rodríguez-Crespo, I., Menéndez, M., García, P., Tateno, H., Goldstein, I. J., Pérez-Agote, B., and Mancheño, J. M. (2011) High-resolution structural insights on the sugar-recognition and fusion tag properties of a versatile β-trefoil lectin domain from the mushroom *Laetiporus sulphureus*. *Glycobiology* **21,** 1349–1361

40. Sánchez-Ruiloba, L., Aicart-Ramos, C., García-Guerra, L., Pose-Utrilla, J., Rodríguez-Crespo, I., and Iglesias, T. (2014) Protein kinase D interacts with neuronal nitric oxide synthase and phosphorylates the activatory residue serine 1412. *PLoS One* **9,** e95191

41. Navarro-Lérida, I., Martínez-Moreno, M., Ventoso, I., Alvarez-Barrientos, A., and Rodríguez-Crespo, I. (2007) Binding of CAP70 to inducible nitric oxide synthase and implications for the vectorial release of nitric oxide in polarized cells. *Mol. Biol. Cell* **18,** 2768–2777

42. Merino-Gracia, J., Costas-Insua, C., Canales, M. Á., and Rodríguez-Crespo, I. (2016) Insights into the C-terminal peptide binding specificity of the PDZ domain of neuronal nitric-oxide synthase: characterization of the interaction with the tight junction protein claudin-3. *J. Biol. Chem.* **291,** 11581–11595

43. Navarro-Lérida, I., Alvarez-Barrientos, A., and Rodríguez-Crespo, I. (2006) N-terminal palmitoylation within the appropriate amino acid environment conveys on NOS2 the ability to progress along the intracellular sorting pathways. *J. Cell Sci.* **119,** 1558–1569

44. Wishart, D. S., Bigam, C. G., Yao, J., Abildgaard, F., Dyson, H. J., Oldfield, E., Markley, J. L., and Sykes, B. D. (1995) ^{1}H, ^{13}C and ^{15}N chemical shift referencing in biomolecular NMR. *J. Biomol. NMR* **6,** 135–140

45. Whitehead, B., Craven, C. J., and Waltho, J. P. (1997) Double and triple resonance NMR methods for protein assignment. *Methods Mol. Biol.* **60,** 29–52

46. Goddard, T. D., and Kneller, D. G. (2005) *Sparky 3*, University of California, San Francisco

47. Güntert, P. (2004) Automated NMR structure calculation with CYANA. *Methods Mol. Biol.* **278,** 353–378

48. Shen, Y., Delaglio, F., Cornilescu, G., and Bax, A. (2009) TALOS+: a hybrid method for predicting protein backbone torsion angles from NMR chemical shifts. *J. Biomol. NMR* **44,** 213–223

49. Case, D. A., Cheatham, T. E., 3rd, Darden, T., Gohlke, H., Luo, R., Merz, K. M., Jr, Onufriev, A., Simmerling, C., Wang, B., and Woods, R. J. (2005) The Amber biomolecular simulation programs. *J. Comput. Chem.* **26,** 1668–1688

50. Laskowski, R. A., Rullmann, J. A., MacArthur, M. W., Kaptein, R., and Thornton, J. M. (1996) AQUA and PROCHECK-NMR: programs for checking the quality of protein structures solved by NMR. *J. Biomol. NMR* **8,** 477–486

51. Koradi, R., Billeter, M., and Wüthrich, K. (1996) MOLMOL: a program for display and analysis of macromolecular structures. *J. Mol. Graph.* **14,** 51–55, 29–32

52. Cook, S. P., Galve-Roperh, I., Martínez del Pozo, A., and Rodríguez-Crespo, I. (2002) Direct calcium binding results in activation of brain serine racemase. *J. Biol. Chem.* **277,** 27782–27792

53. Martínez-Moreno, M., Navarro-Lérida, I., Roncal, F., Albar, J. P., Alonso, C., Gavilanes, F., and Rodríguez-Crespo, I. (2003) Recognition of novel viral sequences that associate with the dynein light chain LC8 identified through a pepscan technique. *FEBS Lett.* **544,** 262–267

54. Rodríguez-Crespo, I., Yélamos, B., Roncal, F., Albar, J. P., Ortiz de Montellano, P. R., and Gavilanes, F. (2001) Identification of novel cellular proteins that bind to the LC8 dynein light chain using a pepscan technique. *FEBS Lett.* **503,** 135–141